

Cite this: *Chem. Sci.*, 2017, **8**, 680Received 5th August 2016  
Accepted 10th September 2016

DOI: 10.1039/c6sc03500k

www.rsc.org/chemicalscience

## Aromatic sulfonation with sulfur trioxide: mechanism and kinetic model†

Samuel L. C. Moors,<sup>\*a</sup> Xavier Deraet,<sup>a</sup> Guy Van Assche,<sup>b</sup> Paul Geerlings<sup>a</sup> and Frank De Proft<sup>a</sup>

Electrophilic aromatic sulfonation of benzene with sulfur trioxide is studied with *ab initio* molecular dynamics simulations in gas phase, and in explicit noncomplexing ( $\text{CCl}_3\text{F}$ ) and complexing ( $\text{CH}_3\text{NO}_2$ ) solvent models. We investigate different possible reaction pathways, the number of  $\text{SO}_3$  molecules participating in the reaction, and the influence of the solvent. Our simulations confirm the existence of a low-energy concerted pathway with formation of a cyclic transition state with two  $\text{SO}_3$  molecules. Based on the simulation results, we propose a sequence of elementary reaction steps and a kinetic model compatible with experimental data. Furthermore, a new alternative reaction pathway is proposed in complexing solvent, involving two  $\text{SO}_3$  and one  $\text{CH}_3\text{NO}_2$ .

## Introduction

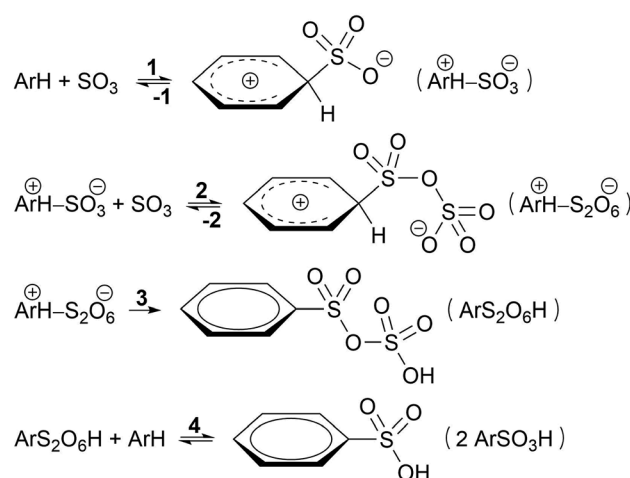
Aromatic sulfonation is a very important chemical transformation of organic compounds.<sup>1,2</sup> It belongs to the well-known class of electrophilic aromatic substitution ( $\text{S}_{\text{E}}\text{Ar}$ ) reactions alongside nitration, halogenation, acylation and alkylolation. Sulfonation is a key reaction step in large industrial applications including pharmaceuticals, detergents, surfactants, dyes, and pesticides.<sup>3–5</sup> The most commonly used sulfonating agents are sulfur trioxide ( $\text{SO}_3$ ), oleum, sulfuric acid and chlorosulfuric acid.<sup>6</sup>

Traditionally,  $\text{S}_{\text{E}}\text{Ar}$  reactions are explained by a two-step  $\text{S}_{\text{E}2}$  or arenium ion mechanism.<sup>7</sup> In the first and rate-determining step, an electrophile attacks the electron-rich aromatic ring to form a  $\sigma$ -complex or wheland or arenium ion intermediate, which is stabilized by mesomery. Aromaticity is restored in the second step by elimination of  $\text{H}^+$ . Recently, alternative pathways to the arenium mechanism have been proposed by Schleyer and coworkers in various electrophilic aromatic substitution reactions<sup>8</sup> including halogenation,<sup>9,10</sup> nitration,<sup>11</sup> and sulfonation.<sup>12</sup> These studies highlight the diversity in reaction mechanisms for  $\text{S}_{\text{E}}\text{Ar}$  and their dependence on substrate and reaction conditions.

Based on kinetic experiments on chlorobenzene and 1,4-dichlorobenzene, Cerfontain and coworkers proposed a three-step kinetic scheme for the sulfonation of arenes with  $\text{SO}_3$  in aprotic solvents (Scheme 1).<sup>13–16</sup> The first step is a reversible

reaction wherein a  $\sigma$ -complex is formed between the arene and a  $\text{SO}_3$  molecule. In the second step a second  $\text{SO}_3$  reversibly binds to the first  $\text{SO}_3$ . Finally, proton transfer from the arene to the second  $\text{SO}_3$  in the third step restores aromaticity and drives the reaction toward arenepyrosulfonic acid ( $\text{ArS}_2\text{O}_6\text{H}$ ), which can be readily hydrolyzed in aqueous media. In apolar noncomplexing  $\text{CCl}_3\text{F}$  solvent sulfonation kinetics are first order in  $\text{SO}_3$ , and thus step 1 was thought to be rate-limiting.<sup>17</sup> In contrast, in polar  $\text{SO}_3$ -complexing<sup>18</sup>  $\text{CH}_3\text{NO}_2$  the rate is second order in  $\text{SO}_3$ , and step 2 was taken as the rate-limiting step.<sup>17</sup>

If less than two equivalents of  $\text{SO}_3$  are used per mole arene, two sulfonation stages can be distinguished. A fast primary stage purportedly proceeds *via* the reaction steps 1–3 (Scheme 1). A much slower secondary stage was proposed to



Scheme 1 Kinetic model proposed by Cerfontain and coworkers for sulfonation with  $\text{SO}_3$ .

<sup>a</sup>Eenheid Algemene Chemie (ALGC), Vrije Universiteit Brussel (VUB), Pleinlaan 2, 1050 Elsene, Brussels, Belgium. E-mail: samuel.moors@vub.ac.be

<sup>b</sup>Physical Chemistry and Polymer Science (FYSC), Vrije Universiteit Brussel (VUB), Pleinlaan 2, 1050 Elsene, Brussels, Belgium

† Electronic supplementary information (ESI) available. See DOI: 10.1039/c6sc03500k

proceed through a reaction of arenepyrosulfonic acid with arene, forming two molecules of arenesulfonic acid ( $\text{ArSO}_3\text{H}$ , step 4).<sup>13,19</sup> This study, however, is focused on the primary sulfonation stage.

The mechanism proposed by Cefontain and coworkers involving a  $\sigma$ -complex intermediate with one  $\text{SO}_3$  has been challenged by recent theoretical studies. Morley *et al.*<sup>20,21</sup> performed quantum chemical calculations at the Hartree-Fock level on the sulfonation of toluene with  $\text{SO}_3$  in gas phase, and concluded that formation of a toluene- $\text{SO}_3$   $\sigma$ -complex was unlikely due to the high energy change required. Instead, they proposed the initial formation of a toluene- $\cdots\text{SO}_3\cdots\text{SO}_3$   $\pi$ -complex followed by a toluene- $\text{S}_2\text{O}_6$   $\sigma$ -complex with almost the same energy, and a cyclic proton rearrangement yielding toluenepyrosulfonic acid.

Schleyer and coworkers studied the sulfonation of several arenes with static density functional and SCS-MP2 calculations in implicit solvent.<sup>12</sup> The sulfonation of benzene, 1,4-dichlorobenzene, toluene, and naphthalene, in gas phase and in apolar solvent were found to proceed *via* a concerted pathway involving two  $\text{SO}_3$  molecules forming a cyclic  $\sigma$ -complex transition state (TS), without intermediate (Scheme 2). In  $\text{CH}_3\text{NO}_2$ , the cyclic  $\sigma$ -complex became an intermediate state, but with low stability. With only one  $\text{SO}_3$ , no intermediate  $\sigma$ -complex was formed in both solvents, and very high energy barriers were needed for sulfonation.

The absence of an intramolecular primary hydrogen kinetic isotope effect (KIE)<sup>17</sup> led Cefontain and coworkers to conclude that the reaction step involving proton transfer (step 3 in Scheme 1) is not rate-limiting. However, the KIE may also be small if the C-H bond is only partially broken at the TS.<sup>22</sup> In the cyclic transition state structures involving two  $\text{SO}_3$  molecules, as calculated by Schleyer and coworkers,<sup>12</sup> the C-H bond is only slightly elongated at the TS in both  $\text{CCl}_3\text{F}$  (0.08 Å) and  $\text{CH}_3\text{NO}_2$  (0.10 Å at the second TS). The small bond elongations are consistent with ratios  $k_{\text{H}}/k_{\text{D}} = 1.2\text{--}1.3$ , suggesting that step 3 may indeed be rate-limiting.

Importantly however, it is not clear how the participation of two  $\text{SO}_3$  molecules, as suggested previously,<sup>12,21</sup> fits in with the first order rate dependence on the  $\text{SO}_3$  concentration in apolar solvent. Morkovnik and Akopova<sup>23</sup> have proposed an alternative low-barrier mechanism with one  $\text{SO}_3$  in apolar solvent. In their

proposal, a sulfuric acid molecule acts as a catalyst by transferring the proton from benzene to  $\text{SO}_3$  *via* a relay-race mechanism (Scheme 2).

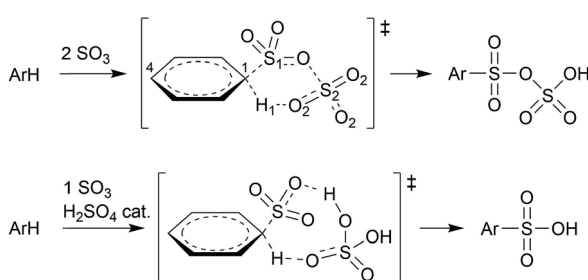
In this study, we aim to further elucidate the reaction mechanism and explain the experimental data. To fully account for solvation and dynamic effects, *ab initio* molecular dynamics (AIMD) is the preferred method of choice. The article is organized as follows. We start with the proposal of a new kinetic model, which is validated by a variety of AIMD simulations in gas phase as well as fully solvated in  $\text{CCl}_3\text{F}$  and  $\text{CH}_3\text{NO}_2$  solvent. Metadynamics (MTD) simulations are performed to study the stability and reactivity of benzene- $\text{SO}_3$  and benzene- $\text{S}_2\text{O}_6$   $\sigma$ -complexes, and to estimate the free energy surface (FES) of the sulfonation reaction. From unbiased MD simulations, we analyze intermolecular interactions between benzene,  $\text{SO}_3$ , and solvent, and we investigate the stability of benzene- $\cdots\text{SO}_3$  and benzene- $\cdots\text{SO}_3\cdots\text{SO}_3$   $\pi$ -complexes in each environment. Finally, restrained MD (rMD) simulations are performed to evaluate the reactivity of the benzene- $\text{S}_2\text{O}_6$   $\sigma$ -complex, and of benzene- $\text{SO}_3 + 1$  catalytic  $\text{H}_2\text{SO}_4$ .

## Results and discussion

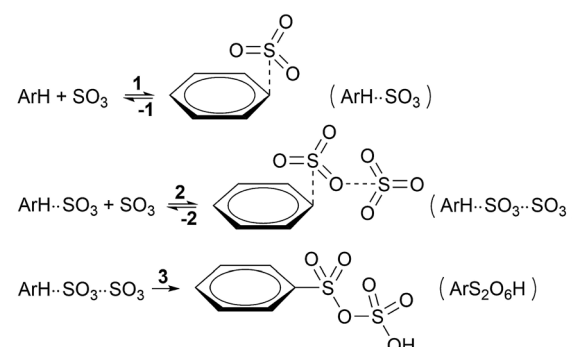
### Mechanism and kinetic model

To enhance readability of the study, we start with the proposal of a new sequence of reaction steps given in Scheme 3 based on our calculation results, which are presented in the following sections, and in agreement with experimental data.

Here, step 1 represents formation of  $\text{ArH}\cdots\text{SO}_3$ , a  $\pi$ -complex between the arene and a first  $\text{SO}_3$  molecule (hereafter named the primary  $\text{SO}_3$ ), step 2 is the formation of the  $\text{ArH}\cdots\text{SO}_3\cdots\text{SO}_3$   $\pi$ -complex between  $\text{ArH}\cdots\text{SO}_3$  and a second  $\text{SO}_3$  (the assisting  $\text{SO}_3$ ), and step 3 is the actual sulfonation reaction with formation of arenepyrosulfonic acid  $\text{ArS}_2\text{O}_6\text{H}$ , the main reaction product. Step 3 requires a significant reorientation of the two  $\text{SO}_3$  molecules toward the plane of the benzene ring to make a cyclic proton rearrangement possible. This mechanism differs from the proposed mechanism of Cefontain and coworkers<sup>13-16</sup> in that it does not account for an intermediate  $\sigma$ -complex state. Although its presence is not ruled out, our simulations confirm previous experimental and theoretical data<sup>12,24</sup> that the stability



Scheme 2 Concerted sulfonation mechanisms in gas phase or apolar solvent with 2  $\text{SO}_3$  molecules according to Schleyer and coworkers,<sup>12</sup> and with 1  $\text{SO}_3 + \text{H}_2\text{SO}_4$  catalyst according to Morkovnik and Akopova.<sup>23</sup>



Scheme 3 New proposed kinetic model for the primary sulfonation stage with  $\text{SO}_3$ .



of  $\sigma$ -complexes is generally low and may be discarded from the kinetic model. Using steady-state conditions, the reaction rate is given by the rate equation (see Appendix):

$$\frac{d(ArS_2O_6H)}{dt} = \frac{k_1 k_2 k_3 [ArH][SO_3]^2}{(k_{-2} + k_3)(k_{-1} + k_2[SO_3])} \quad (1)$$

Depending on the solvent, the reaction may be first order or second order in  $SO_3$ ,<sup>13,14</sup> which dictates limiting condition 1 (Table 1). In apolar  $CCl_3F$  solvent, the reaction is first order in  $SO_3$ , and thus  $k_{-1} \ll k_2[SO_3]$ , which implies that the  $ArH \cdots SO_3$  complex must remain stable long enough that it can associate with an assisting  $SO_3$  before the primary  $SO_3$  dissociates from the arene. In polar  $CH_3NO_2$ , the reaction is second order in  $SO_3$  and  $k_{-1} \gg k_2[SO_3]$ , thus the arene exists as mostly uncomplexed with  $SO_3$ . Whereas the rate-limiting step could in principle be step 1 or 3 in  $CCl_3F$ , and step 2 or 3 in  $CH_3NO_2$  (Table 1, condition 2), our results suggest that (i) the calculated free energy barriers of sulfonation are relatively high, and (ii) the assisting  $SO_3$  detaches rapidly from  $ArH \cdots SO_3 \cdots SO_3$ , which strongly suggests that  $k_{-2} \gg k_3$ , thus step 3 is rate-limiting in both solvents.

In the following sections we validate the proposed mechanism and kinetic model by analyzing a carefully chosen set of advanced AIMD simulations in gas phase and fully solvated in  $CCl_3F$  and  $CH_3NO_2$ .

### Reaction of benzene + 1 $SO_3$

We first examine if a stable  $\sigma$ -complex can be formed between benzene and a single  $SO_3$  molecule, as proposed by Cerfontain and coworkers,<sup>13–16</sup> and if aromatic sulfonation is possible with only 1  $SO_3$ . MTD simulations are performed with one collective variable (CV), the coordination number  $CN_{CS}$  that measures bond formation between a benzene carbon and the  $SO_3$  sulfur. The resulting potential of mean force (PMF) in gas phase, in  $CCl_3F$ , and in  $CH_3NO_2$  is shown in Fig. 1. The benzene $\cdots SO_3$  complex is located at  $CN_{CS} \approx 0.085$  ( $r_{CS} = 2.9 \text{ \AA}$ ). Large free energy differences are observed between the three environments, the  $\sigma$ -complex ( $CN_{CS} \approx 0.5$ –0.6) being most stabilized in the polar  $CH_3NO_2$ . However, no intermediate  $\sigma$ -complex between benzene and  $SO_3$  can be discerned from the PMF, in agreement with previous static calculations.<sup>12</sup>

The MTD simulations are continued by further adding Gaussian hills to the reactant state until reaction. No reaction is observed until a barrier height  $\Delta F^\ddagger \approx 244 \text{ kJ mol}^{-1}$  is reached,

**Table 1** Experimental order in  $SO_3$  (x) in solvents  $CCl_3F$  and  $CH_3NO_2$ , corresponding limiting conditions and rate-limiting step (RLS) derived from eqn (1)

Solvent	$[SO_3]^x$	Condition 1	Condition 2	RLS
$CCl_3F$	1	$k_{-1} \ll k_2[SO_3]$	$k_{-2} \ll k_3$ $k_{-2} \gg k_3$	1 3
$CH_3NO_2$	2	$k_{-1} \gg k_2[SO_3]$	$k_{-2} \ll k_3$ $k_{-2} \gg k_3$	2 3

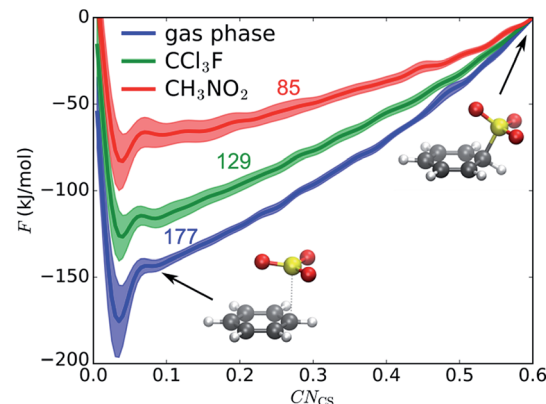


**Fig. 1** Reaction between benzene and 1  $SO_3$  in gas phase,  $CCl_3F$ , and  $CH_3NO_2$ . PMF of 1D MTD with error bars representing the standard deviation. Numbers above the curves indicate free energy  $\Delta F$  ( $\text{kJ mol}^{-1}$ ) of the  $\sigma$ -complex at  $CN_{CS} = 0.6$  relative to the reactant state. Structures refer to the gas phase curve.

which is incompatible with the fast experimental reaction kinetics.<sup>15</sup> In conclusion, the MTD simulations suggest that sulfonation of benzene with a single  $SO_3$  is not a viable pathway, and can be discarded in the kinetic analysis.

### Stability of benzene $\cdots SO_3 \cdots SO_3$ and benzene $\cdots SO_3$ $\pi$ -complexes

To assess the validity of steps 1 and 2 of our kinetic model (Scheme 3), the stability of the  $\pi$ -complexes is studied with a series of independent (different starting structures and velocities) and unbiased AIMD simulations starting from the benzene $\cdots SO_3 \cdots SO_3$  complex. The results are listed in Table 2 and summarized in Fig. 2.

In gas phase, the benzene $\cdots SO_3 \cdots SO_3$  complex remains stable throughout the simulation. A clear distinction can be made between the two interacting  $SO_3$  molecules (Fig. 3a). The first (primary)  $SO_3$  is tightly bound to benzene by strong  $\pi$  interaction between its S atom and the  $\pi$ -conjugated ring system located above the benzene C atoms. The second (assisting)  $SO_3$  is loosely bound to the primary  $SO_3$  and occasionally strays away from the complex, while remaining at the same side of the ring plane most of the time. In both  $CCl_3F$  and  $CH_3NO_2$  solvents, however, one  $SO_3$  dissociates from the complex and drifts into the bulk solvent. The resulting benzene $\cdots SO_3$  complex remains stable in  $CCl_3F$ , whereas in  $CH_3NO_2$  this complex dissociates into solvated benzene and  $SO_3$ .

Overall, the unbiased MD simulations described here show that the benzene $\cdots SO_3 \cdots SO_3$   $\pi$ -complex is stable in gas phase but unstable in both solvents. The benzene $\cdots SO_3$  complex appears relatively stable in  $CCl_3F$ , consistent with the limiting condition  $k_{-1} \ll k_2[SO_3]$  (Table 1), and in agreement with the experimental first order rate in  $SO_3$ . In contrast, strong interactions with  $CH_3NO_2$  solvent shift the equilibrium toward separate benzene and  $SO_3$  reactants, in accord with  $k_{-1} \gg k_2[SO_3]$  (Table 1), in correspondence with the second order rate



Table 2 Overview of MD and rMD simulations

Initial conditions	Environment	$t^a$ (ps)	Reaction <sup>b</sup>
<b>Unbiased MD</b>			
Benzene $\cdots$ SO <sub>3</sub> $\cdots$ SO <sub>3</sub>	Gas phase	120	Remains stable
	CCl <sub>3</sub> F	200	$\rightarrow$ Benzene $\cdots$ SO <sub>3</sub> + SO <sub>3</sub> (30 ps)
		200	$\rightarrow$ Benzene $\cdots$ SO <sub>3</sub> + SO <sub>3</sub> (140 ps)
	CH <sub>3</sub> NO <sub>2</sub>	70	$\rightarrow$ Benzene $\cdots$ SO <sub>3</sub> + SO <sub>3</sub> (30 ps) $\rightarrow$ Benzene + 2 SO <sub>3</sub> (70 ps)
		180	$\rightarrow$ Benzene $\cdots$ SO <sub>3</sub> + SO <sub>3</sub> (60 ps) $\rightarrow$ Benzene + 2 SO <sub>3</sub> (180 ps)
<b>Restrained MD</b>			
Benzene-S <sub>2</sub> O <sub>6</sub>	Gas phase	40	$\rightarrow$ Benzene-S <sub>2</sub> O <sub>6</sub> H
		60	$\rightarrow$ Benzene-S <sub>2</sub> O <sub>6</sub> H
	CCl <sub>3</sub> F	5	$\rightarrow$ Benzene-S <sub>2</sub> O <sub>6</sub> H
		10	$\rightarrow$ Benzene-S <sub>2</sub> O <sub>6</sub> H
Benzene-SO <sub>3</sub> $\cdots$ H <sub>2</sub> SO <sub>4</sub>	CH <sub>3</sub> NO <sub>2</sub>	200	Remains stable
	Gas phase	6	$\rightarrow$ Benzene-SO <sub>3</sub> H $\cdots$ H <sub>2</sub> SO <sub>4</sub>
	CCl <sub>3</sub> F	170	$\rightarrow$ Benzene-SO <sub>3</sub> H $\cdots$ H <sub>2</sub> SO <sub>4</sub>
	CH <sub>3</sub> NO <sub>2</sub>	90	$\rightarrow$ Benzene-SO <sub>3</sub> H $\cdots$ H <sub>2</sub> SO <sub>4</sub>

<sup>a</sup> Total simulation time. <sup>b</sup> Time at which the event takes place is given between parentheses.

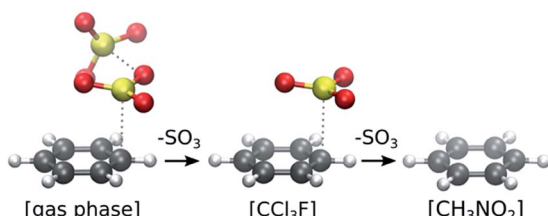


Fig. 2 Stability of  $\pi$ -complexes in different solvation models, showing the decrease in number of SO<sub>3</sub> molecules complexed with benzene.

in SO<sub>3</sub>. In summary, our simulation results suggest that the reactant species is benzene $\cdots$ SO<sub>3</sub> in CCl<sub>3</sub>F and benzene CH<sub>3</sub>NO<sub>2</sub>, in agreement with steps 1 and 2 of our kinetic model (Scheme 3).

### Specific solvation of reactants

The low stability of the benzene $\cdots$ SO<sub>3</sub>  $\pi$ -complex in CH<sub>3</sub>NO<sub>2</sub> is attributed to specific solvent interactions. Electrostatic interaction between the positively charged S atom of SO<sub>3</sub> and the negatively charged O atoms of CH<sub>3</sub>NO<sub>2</sub> strongly increases upon dissociation of the complex. This solvent interaction is demonstrated in Fig. 3b by the red probability isosurface of CH<sub>3</sub>NO<sub>2</sub> O atoms around SO<sub>3</sub>, where larger volumes indicate a higher probability of finding an O atom inside the isosurface. Likewise, electrostatic interactions between the benzene  $\pi$  electron cloud and the positively charged methyl group of CH<sub>3</sub>NO<sub>2</sub> (grey), and between the positively charged H atoms of benzene and the O atoms of CH<sub>3</sub>NO<sub>2</sub> (red) markedly increase upon dissociation (Fig. 3c).

### Reaction of benzene + 2 SO<sub>3</sub>

The sulfonation reaction starting from the benzene $\cdots$ SO<sub>3</sub> $\cdots$ SO<sub>3</sub>  $\pi$ -complex, corresponding to step 3 in our kinetic model (Scheme 3), is investigated with MTD and two collective

variables, CN<sub>CS</sub> and CN<sub>CO</sub>; the latter is the coordination between a benzene C and the O atom of the assisting SO<sub>3</sub>. In Fig. 4a–c, the resulting 2D FES is shown as the average of three

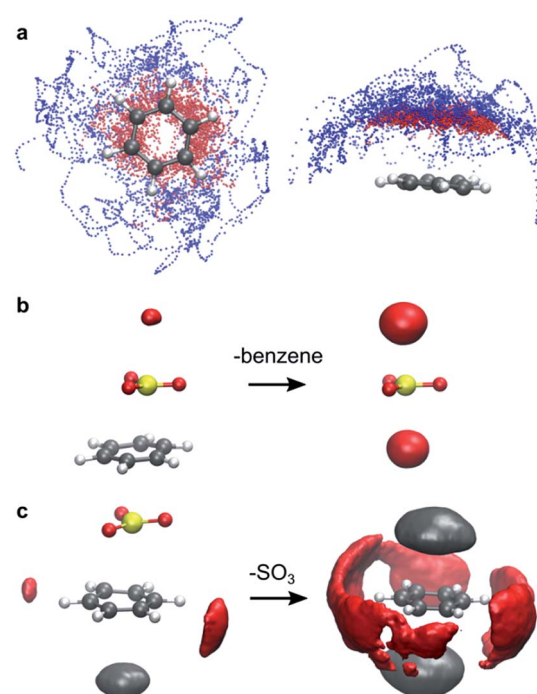


Fig. 3 Intermolecular interactions observed during AIMD simulations. (a) Benzene-SO<sub>3</sub> interactions in gas phase. Superposition of snapshots of the benzene $\cdots$ SO<sub>3</sub> $\cdots$ SO<sub>3</sub> complex in top view (left) and side view (right). Dots represent the S atom positions of the primary SO<sub>3</sub> (red) and assisting SO<sub>3</sub> (blue). (b) Specific SO<sub>3</sub> $\cdots$ CH<sub>3</sub>NO<sub>2</sub> interactions. Probability isosurface (red) of CH<sub>3</sub>NO<sub>2</sub> O atoms around the SO<sub>3</sub> S atom in a benzene $\cdots$ SO<sub>3</sub> complex (left) and in separated SO<sub>3</sub> (right). (c) Specific benzene $\cdots$ CH<sub>3</sub>NO<sub>2</sub> interactions. Probability isosurface of solvent O (red) and C (grey) atoms around benzene C atoms, in a benzene $\cdots$ SO<sub>3</sub> complex (left) and in separated benzene (right). Deviations from symmetry in the isosurfaces are due to finite sampling.



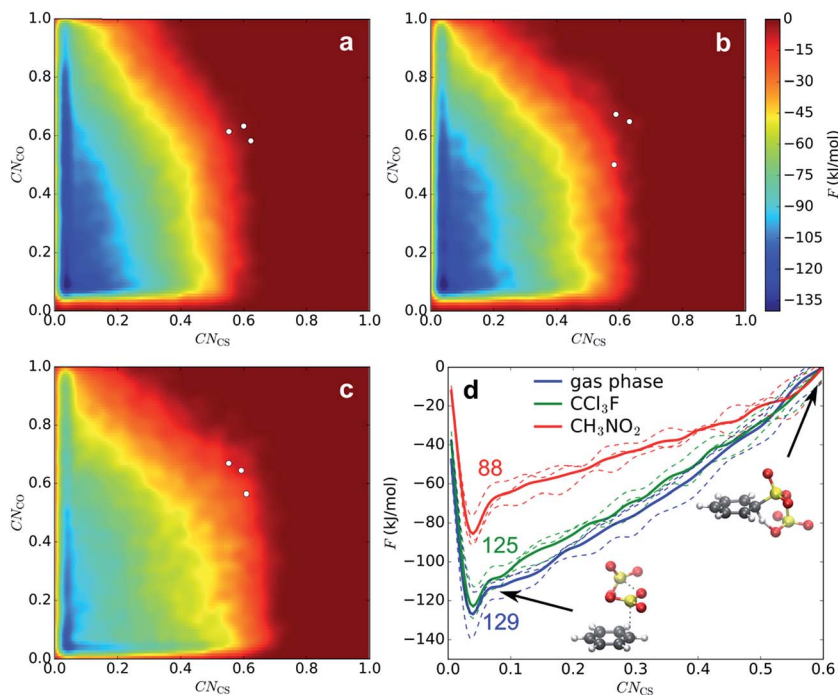


Fig. 4 FES of 2D MTD in gas phase (a),  $\text{CCl}_3\text{F}$  (b), and  $\text{CH}_3\text{NO}_2$  (c), and corresponding projected PMFs along  $\text{CN}_{\text{CS}}$  (d). The given numbers indicate average  $\Delta F^\ddagger$  values ( $\text{kJ mol}^{-1}$ ).

MTD simulations. Again, no intermediate  $\sigma$ -complex is observed in the three environments. The surface is very similar in gas phase and  $\text{CCl}_3\text{F}$ , whereas in  $\text{CH}_3\text{NO}_2$  the reactant valley is much shallower due to stabilization of TS by the electrostatic field. The position of TS, as indicated with white dots, is similar in the three environments:  $\text{CV1} \cong \text{CV2} \cong 0.6$ , which corresponds to a cyclic transition state with two  $\text{SO}_3$  molecules at  $r_{\text{CS}} \cong 1.84 \text{ \AA}$  and  $r_{\text{CO}} \cong 2.7\text{--}3.2 \text{ \AA}$ . In all cases benzene pyrosulfonic acid is formed in one step. In contrast to  $\text{CV1}$ , the free energy change along the  $\text{CV2}$  axis is small. After projecting  $\text{CV2}$  onto  $\text{CV1}$ , a 1D PMF is obtained (Fig. 4d). Mean geometric parameters at TS are shown in Table S2 (ESI†).

Low-temperature MD of the  $\sigma$ -complex in  $\text{CH}_3\text{NO}_2$  shows that a metastable intermediate state may exist nonetheless (see ESI†). The stability of the  $\sigma$ -complex is however very low, which may in part be due to the BLYP density functional used in this study. Low stabilities of the intermediate state ( $2\text{--}4 \text{ kJ mol}^{-1}$ ) have also been calculated previously at the M06-2X/6-311+G(2d,2p) level for benzene and 1,4-dichlorobenzene in implicit  $\text{CH}_3\text{NO}_2$ .<sup>12</sup>

### Reactivity of benzene- $\text{S}_2\text{O}_6$ $\sigma$ -complex

Although we have now established that  $\sigma$ -complexes of benzene and  $\text{SO}_3$  are fairly unstable, it is insightful to analyze the benzene- $\text{SO}_3$  interactions in the  $\sigma$ -complex state and to monitor the influence of the environment on their reactivity toward benzene- $\text{S}_2\text{O}_6\text{H}$  formation. Additionally, the obtained reactivity information will allow us to decompose the free energy barrier into several discrete contributions.

Restrained MD (rMD) simulations are performed of the benzene- $\text{SO}_3$   $\sigma$ -complex + an assisting  $\text{SO}_3$ , which forms a benzene- $\text{S}_2\text{O}_6$   $\sigma$ -complex. To stabilize the  $\sigma$ -complex, the  $\text{C}_1\text{--S}_1$  bond is restrained with a harmonic potential, which keeps  $\text{CN}_{\text{CS}}$  between 0.5 and 0.6 until sulfonation takes place. The results are summarized in Table 2. In gas phase (40–60 ps) and in  $\text{CCl}_3\text{F}$  solvent (5–10 ps), a concerted sulfonation reaction takes place by proton transfer to the assisting  $\text{SO}_3$  with formation of benzene pyrosulfonic acid in one step (Fig. 5). In  $\text{CH}_3\text{NO}_2$  solvent, however, no product formation is observed during 200 ps. Two factors contribute to the increased stability of the  $\sigma$ -complex in  $\text{CH}_3\text{NO}_2$ : (i) stabilization of the zwitterionic TS by the strong solvent electrostatic field, and (ii) competition with the solvent for hydrogen bonding with  $\text{H}_1$ . The latter effect is demonstrated in Fig. 6a, showing a stable intramolecular  $\text{O}_2\text{--H}_1$

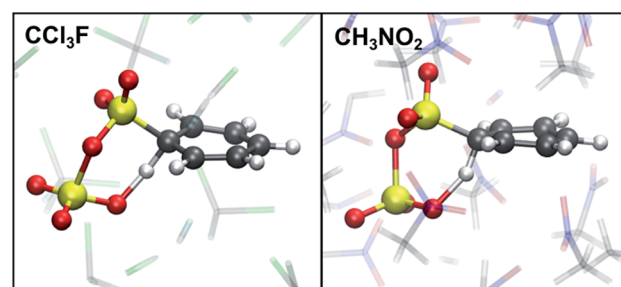


Fig. 5 TS of sulfonation of benzene with 2  $\text{SO}_3$ . In  $\text{CCl}_3\text{F}$ , the reaction takes place spontaneously during rMD. In  $\text{CH}_3\text{NO}_2$  an additional barrier needs to be crossed with rMTD. Atom colors are: C (grey), Cl (green), F (cyan), H (white), N (blue), O (red), S (yellow).



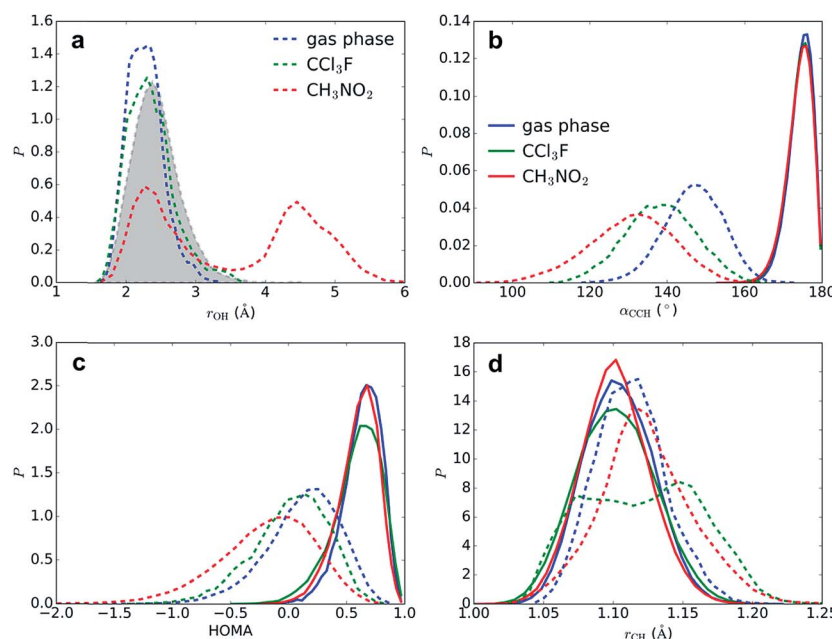


Fig. 6 Geometric probability densities ( $P$ ) in reactant state (benzene- $\cdots\text{SO}_3$   $\pi$ -complex, full lines) and close to TS (benzene- $\text{S}_2\text{O}_6$   $\sigma$ -complex, dashed lines), in gas phase (blue),  $\text{CCl}_3\text{F}$  (green), and  $\text{CH}_3\text{NO}_2$  (red). (a) minimal distance  $r(\text{H}_1-\text{O}_2)$  and minimal distance  $r(\text{H}_1-\text{O})$  with  $\text{CH}_3\text{NO}_2$  (filled grey), (b) angle  $\alpha(\text{C}_4-\text{C}_1-\text{H}_1)$ , (c) HOMA aromaticity index, (d) distance  $r(\text{C}_1-\text{H}_1)$ .

hydrogen bond in gas phase and  $\text{CCl}_3\text{F}$ , whereas in  $\text{CH}_3\text{NO}_2$  this hydrogen bond is present only  $\sim 50\%$  of the time.

### Solvation effects at the transition state

The segments of rMD trajectories before reaction are analyzed to determine how the transition state geometry is affected by solvation effects. The effects of the solvent on benzene geometry near TS are striking (Fig. 6b-d). The angle  $\alpha(\text{C}_4-\text{C}_1-\text{H}_1)$  is calculated as a measure for the degree of  $\text{sp}^3$  hybridization at  $\text{C}_1$  and thus the stability of the  $\sigma$ -complex. In the reactant state, the mean angle  $\langle\alpha\rangle = 174^\circ$  in all three environments, indicating that  $\text{H}_1$  is located mostly in the plane of the benzene ring and hence  $\text{C}_1$  is almost purely  $\text{sp}^2$  hybridized, whereas near TS  $\text{C}_1$  displays strong  $\text{sp}^3$  character. The smallest  $\langle\alpha\rangle$  is measured in  $\text{CH}_3\text{NO}_2$  ( $131^\circ$ ), followed by  $\text{CCl}_3\text{F}$  ( $138^\circ$ ) and gas phase ( $147^\circ$ ). The strong stabilizing effect of  $\text{CCl}_3\text{F}$  is remarkable given its low polarity. The harmonic oscillator model of aromaticity index (HOMA)<sup>25</sup> fluctuates around a mean value  $\langle\text{HOMA}\rangle = 0.59-0.63$  in the reactant state, but degrades near TS, indicating nearly complete loss of aromaticity. This effect is especially strong in  $\text{CH}_3\text{NO}_2$  ( $\langle\text{HOMA}\rangle = -0.19$ ), in comparison with  $\text{CCl}_3\text{F}$  (0.02) and gas phase (0.13). The  $\text{C}_1-\text{H}_1$  bond is stretched from  $\langle r_{\text{CH}} \rangle = 1.102-1.104$  Å to 1.124, 1.121, and 1.113 Å in  $\text{CH}_3\text{NO}_2$ ,  $\text{CCl}_3\text{F}$ , and gas phase, respectively. In  $\text{CCl}_3\text{F}$ , a bimodal distribution is observed due to frequent near-proton transfer events taking place.

### An alternative pathway in $\text{CH}_3\text{NO}_2$

An estimate of the additional free energy barrier required for sulfonation of the benzene- $\text{S}_2\text{O}_6$   $\sigma$ -complex in  $\text{CH}_3\text{NO}_2$  is

obtained with restrained MTD (rMTD) (for computational details and PMFs, see ESI†), yielding an average additional  $\Delta F = 12$  kJ mol<sup>-1</sup>. In one of the rMTD runs, an alternative pathway is observed (Fig. 7). First, the C-H bond is weakened by hydrogen bonding interaction with the assisting  $\text{SO}_3$ , which strongly lowers the activation free energy of proton transfer. Next, the proton is transferred to a nitromethane molecule (224 fs, TS1). Shortly thereafter, the proton is transferred from nitromethane to the primary  $\text{SO}_3$  to form benzenesulfonic acid

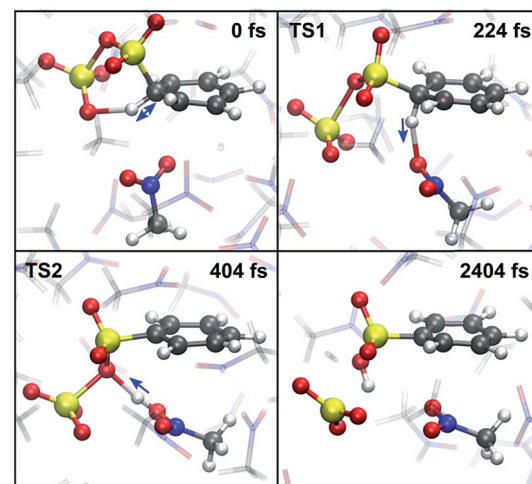


Fig. 7 Snapshots of the new  $\text{CH}_3\text{NO}_2$ -mediated sulfonation pathway. (0 fs)  $\text{H}_1-\text{O}_2$  hydrogen bond at maximal strength. (224 fs) TS1: proton transfer from benzene to  $\text{CH}_3\text{NO}_2$ . (404 fs) TS2: proton transfer from  $\text{CH}_3\text{NO}_2$  to the primary  $\text{SO}_3$ . (2404 fs) stable benzenesulfonic acid product. Blue arrows indicate the direction of motion of the proton.

(404 fs, TS2). Thus, although in this mechanism the assisting  $\text{SO}_3$  is not the proton acceptor, it still plays an essential role in the reaction by activating the  $\text{C}_1\text{-H}_1$  bond. The calculated additional free energy barrier for this pathway  $\Delta F^\ddagger = 14 \text{ kJ mol}^{-1}$ , suggesting that this new mechanism is feasible and may compete with the cyclic proton transfer pathway.

### Free energy decomposition

Combining the results of 1D and 2D MTD and the rMD simulations, the total  $\Delta F^\ddagger$  can be decomposed into three contributions: (1) benzene- $\cdots\text{SO}_3$   $\pi$ -complex to benzene- $\text{SO}_3$   $\sigma$ -complex, (2) benzene- $\text{SO}_3$   $\sigma$ -complex to benzene- $\text{S}_2\text{O}_6$   $\sigma$ -complex, and (3) benzene- $\text{S}_2\text{O}_6$  to TS. In gas phase, the presence of an assisting  $\text{SO}_3$  strongly reduces the free energy required to form a  $\sigma$ -complex from the  $\pi$ -complex (177 to 129  $\text{kJ mol}^{-1}$ ). Once the benzene- $\text{S}_2\text{O}_6$   $\sigma$ -complex is formed, sulfonation proceeds spontaneously. In  $\text{CCl}_3\text{F}$ , the assisting  $\text{SO}_3$  has a slight stabilizing effect on the  $\sigma$ -complex (129 to 125  $\text{kJ mol}^{-1}$ ). In  $\text{CH}_3\text{NO}_2$ , the solvent already has a strong stabilizing effect, which causes the additional stabilizing effect of the assisting  $\text{SO}_3$  to be rather small (85 to 76  $\text{kJ mol}^{-1}$ ). The combined stabilizing effects lead to an additional free energy barrier required for sulfonation (76 + 12 = 88  $\text{kJ mol}^{-1}$ ).

### $\text{H}_2\text{SO}_4$ as a catalyst

As an alternative explanation for the first-order reaction in  $\text{SO}_3$  in noncomplexing media, Morkovnik and Akopova suggested a relay-race mechanism involving a Brønsted acid as a catalyst (Scheme 2).<sup>23</sup> The plausibility of this mechanism is verified with rMD simulations of the benzene- $\text{SO}_3$   $\sigma$ -complex, restrained at the  $\text{C}_1\text{-S}_1$  bond, in the presence of a  $\text{H}_2\text{SO}_4$  molecule. Spontaneous sulfonation takes place in all three environments within 170 ps (Table 2), although the mechanism differs from the mechanism proposed previously<sup>23</sup> and depends on the polarity

of the environment (Fig. 8). In gas phase and  $\text{CCl}_3\text{F}$ ,  $\text{H}_1$  is first transferred from benzene to  $\text{H}_2\text{SO}_4$  at TS1, stabilized by one (gas phase) or two ( $\text{CCl}_3\text{F}$ )  $\text{H}_2\text{SO}_4\cdots\text{SO}_3$  hydrogen bonds. Proton transfer from  $\text{H}_2\text{SO}_4$  to  $\text{SO}_3$  follows quickly thereafter (TS2, 16 fs). In  $\text{CH}_3\text{NO}_2$ , first proton transfer occurs from  $\text{H}_2\text{SO}_4$  to  $\text{SO}_3$  (TS1), followed by benzene-to- $\text{H}_2\text{SO}_4$  proton transfer 106 fs later (TS2). We conclude that catalytic amounts of  $\text{H}_2\text{SO}_4$  in  $\text{CCl}_3\text{F}$  may provide an alternative pathway consistent with first-order kinetics in  $\text{SO}_3$ , however the participation of  $\text{H}_2\text{SO}_4$  is not required in our kinetic model. In  $\text{CH}_3\text{NO}_2$ , the stability of the benzene- $\cdots\text{SO}_3\cdots\text{H}_2\text{SO}_4$   $\pi$ -complex is probably too low to meaningfully contribute to the overall reaction.

### Conclusions

The mechanism and kinetics of electrophilic aromatic sulfonation have been investigated in great detail with various DFT-based first-principles MD and MTD simulations. Three different environments were compared: gas phase, and fully solvated in explicit apolar ( $\text{CCl}_3\text{F}$ ) and polar ( $\text{CH}_3\text{NO}_2$ ) solvents. Several alternative reaction mechanisms were evaluated, including with 1 or 2  $\text{SO}_3$  molecules, with a catalytic  $\text{H}_2\text{SO}_4$  molecule, and with a participating solvent molecule. The kinetic model proposed by Cerfontain and coworkers, involving stable  $\text{ArH-SO}_3$  and  $\text{ArH-S}_2\text{O}_6$   $\sigma$ -complexes in step 1 and 2, was examined. Our results suggest that both benzene- $\text{SO}_3$  and benzene- $\text{S}_2\text{O}_6$   $\sigma$ -complexes are unstable at room temperature, thus ruling out the Cerfontain model. Our simulation data confirm the static gas phase and implicit solvent calculations performed by Schleyer and coworkers, which suggest that the free energy barrier for sulfonation with a single  $\text{SO}_3$  is too high to be feasible. In all three environments, a low-energy concerted pathway starting from the benzene- $\cdots\text{SO}_3\cdots\text{SO}_3$   $\pi$ -complex was found, involving a cyclic transition state with proton transfer from benzene to the assisting  $\text{SO}_3$ , and with formation of benzene pyrosulfonic acid. This mechanism is in agreement with the calculations of Schleyer and coworkers, although in  $\text{CH}_3\text{NO}_2$  an intermediate cyclic  $\sigma$ -complex state with low stability was found by them.

In order to bring the concerted mechanism into agreement with experimental kinetic data, a new kinetic model was proposed. Steps 1 and 2 represent the formation of  $\text{ArH-SO}_3$  and  $\text{ArH-SO}_3\cdots\text{SO}_3$   $\pi$ -complexes, respectively, followed by cyclic proton transfer with formation of benzene pyrosulfonic acid in step 3. A rate equation was calculated using the steady-state approximation, and the limiting conditions were determined on the basis of the experimental rate order in  $\text{SO}_3$ . In  $\text{CCl}_3\text{F}$  we found that  $k_{-1} \ll k_2[\text{SO}_3]$ , whereas in  $\text{CH}_3\text{NO}_2$  the opposite condition  $k_{-1} \ll k_2[\text{SO}_3]$  applies. The validity of steps 1 and 2 was confirmed with long timescale MD simulations, suggesting that the benzene- $\cdots\text{SO}_3$   $\pi$ -complex is relatively stable in  $\text{CCl}_3\text{F}$  but quickly dissociates in  $\text{CH}_3\text{NO}_2$ . The mechanism suggested by Morkovnik and Akopova involving one  $\text{SO}_3$  and a catalytic  $\text{H}_2\text{SO}_4$  molecule was shown to provide a viable alternative route to sulfonation in  $\text{CCl}_3\text{F}$ . Furthermore, a new and unanticipated mechanism was discovered in  $\text{CH}_3\text{NO}_2$ , in which two  $\text{SO}_3$  and one  $\text{CH}_3\text{NO}_2$  cooperate in a stepwise proton transfer from benzene to  $\text{CH}_3\text{NO}_2$ , followed by proton transfer

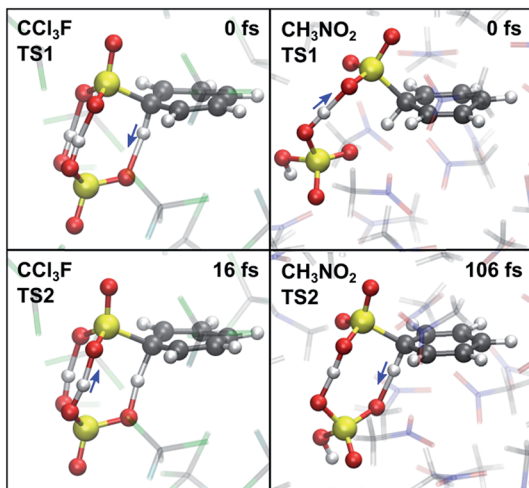


Fig. 8 TS1 (top) and TS2 (bottom) in the presence of catalytic  $\text{H}_2\text{SO}_4$ , corresponding to the first and second proton transfer in  $\text{CCl}_3\text{F}$  (left) and  $\text{CH}_3\text{NO}_2$  (right).



to the primary  $\text{SO}_3$ , leading directly to benzenesulfonic acid. Future research will focus on sulfonation of substituted benzenes and benzene derivatives with  $\text{SO}_3$  to investigate whether our kinetic model is applicable to a wide range of arenes.

## Computational methods

### Molecular dynamics

Born–Oppenheimer molecular dynamics simulations are performed at the DFT level with the gradient-corrected BLYP functional,<sup>26,27</sup> the DZVP-GTH basis set,<sup>28</sup> and Grimme D3 dispersion corrections.<sup>29</sup> The BLYP functional has been shown to produce barriers for  $\text{SN}_2$  and  $\text{E}_2$  reactions in good agreement with high-level (MP2) calculations.<sup>30</sup> The integration time step is set at 1 fs, with snapshots taken every 2 fs. Simulations in solvent are performed in the NVT ensemble, using the canonical sampling through velocity rescaling thermostat<sup>31</sup> with a time constant of 50 fs. The reactants are placed inside a periodic cubic box filled with 25  $\text{CCl}_3\text{F}$  or 40  $\text{CH}_3\text{NO}_2$  molecules. The densities are set to the experimental densities of  $\text{CCl}_3\text{F}$  (1.48 g ml<sup>-1</sup>) and  $\text{CH}_3\text{NO}_2$  (1.13 g ml<sup>-1</sup>) at 298 K, with corresponding box lengths 15.847/15.911 Å ( $\text{CCl}_3\text{F}$ ) and 15.482/15.549 Å ( $\text{CH}_3\text{NO}_2$ ), depending on the number of  $\text{SO}_3$  molecules present. All AIMD simulations are performed with the CP2K simulation package (version 2.6).<sup>32</sup>

### Metadynamics

Most chemical reactions are not accessible in the timescale (typically < 1 ns) that can be reached with AIMD. In order to sample the relevant TS regions, enhanced sampling techniques need to be used. Metadynamics is a nonequilibrium MD method introduced by Laio and Parrinello.<sup>33,34</sup> In recent studies, we have successfully used the MTD technique to estimate free energy surfaces in a variety of systems, including heterogeneous catalysis and reactions in solution.<sup>35–37</sup> Sampling is advanced by adding Gaussian potential hills along a limited number of carefully chosen collected variables during the simulation, effectively flattening the FES by filling low-energy regions. The FES is then calculated as the opposite of the summation of the Gaussian hills.

The hills are added every 25 steps along one or two collective variables (CVs), defined by coordination numbers CN:

$$\text{CN} = \sum_{i,j} \frac{1 - (r_{ij}/r_0)^6}{1 - (r_{ij}/r_0)^{12}} \quad (2)$$

where the sum runs over two nonoverlapping sets of atoms  $i$  and  $j$ ,  $r_{ij}$  is the distance between atoms  $i$  and  $j$ , and  $r_0$  is a reference distance. CV1 is described by  $\text{CN}_{\text{CS}}$  between a benzene  $\text{C}_1$  and  $\text{S}_1$  (see Scheme 2 for atom numbering), with  $r_0 = 1.964$  Å. In the 2D MTD simulations, CV2 corresponds to  $\text{CN}_{\text{CO}}$ , the sum of coordination numbers between  $\text{C}_1$  and the three  $\text{O}_2$  atoms, with  $r_0 = 2.719$  Å. The width of the hills is set to 0.02. In the 1D MTD simulations, the hill height is initially set to  $H = 1$  kJ mol<sup>-1</sup>, and reduced to 0.5 kJ mol<sup>-1</sup> after 40 ps. In the 2D MTD,  $H = 2$  kJ mol<sup>-1</sup>. To limit sampling to a region close to the bound

state, half harmonic bias potentials are added to CV1 and CV2 at position 0.03 with a force constant  $K_f = 100$  a.u. In the 2D MTD, an additional half harmonic potential is added to the  $\text{S}_1\text{--S}_2$  distance at 4.5 Å with  $K_f = 0.19$  a.u. The MTD simulations are ended once the product state is reached. To dampen excessive proton fluctuations, the mass of  $\text{H}_1$  is increased to that of tritium.

In the 2D MTD, Gaussian hills are placed along two CVs simultaneously:  $\text{CN}_{\text{CS}}$  and  $\text{CN}_{\text{CO}}$ , which allows for a sulfonation with either one or two  $\text{SO}_3$  molecules. Due to the involvement of proton transfer, however, it is impossible to simulate the reaction in the conventional way, *i.e.* sampling many forward and reverse reactions by filling both the reactant and product wells with Gaussian hills. Instead, three independent MTD simulations are initiated from different starting geometries and terminated as soon as the proton transfer has taken place. The TS is then taken as the last stationary point along the  $r_{\text{CH}}$  trajectory before proton transfer takes place.

### Analysis

Probability isosurfaces are calculated with the volmap tool of VMD.<sup>38</sup> The probability isosurface of  $\text{CH}_3\text{NO}_2$  O atoms within 4 Å of the  $\text{SO}_3$  S atom is calculated with isovalue = 65%. Probability isosurfaces of  $\text{CH}_3\text{NO}_2$  O and C atoms within 4 Å of any of the six benzene C atoms are calculated with isovalue = 30%. Conversion of the 2D FES into a 1D PMF is achieved by projecting CV2 onto CV1, and free energy barriers are calculated as the free energy difference between the TS and the reactant state.<sup>36</sup>

## Appendix

Here we derive the rate equation (eqn (1)). Let  $\text{A} = \text{ArH}$ ,  $\text{B} = \text{SO}_3$ ,  $\text{C} = \text{ArH}\cdots\text{SO}_3$ ,  $\text{D} = \text{ArH}\cdots\text{SO}_3\cdots\text{SO}_3$ ,  $\text{E} = \text{ArS}_2\text{O}_6\text{H}$ . Using the steady-state approximation, we have

$$\frac{d[\text{C}]}{dt} = k_1[\text{A}][\text{B}] - k_{-1}[\text{C}] - k_2[\text{B}][\text{C}] = 0 \quad (3)$$

$$\frac{d[\text{D}]}{dt} = k_2[\text{B}][\text{C}] - k_{-2}[\text{D}] - k_3[\text{D}] = 0 \quad (4)$$

From eqn (3)–(4):

$$[\text{D}] = \frac{k_1 k_2 [\text{A}][\text{B}]^2}{(k_{-2} + k_3)(k_{-1} + k_2[\text{B}])} \quad (5)$$

$$\frac{d[\text{E}]}{dt} = k_3[\text{D}] = \frac{k_1 k_2 k_3 [\text{A}][\text{B}]^2}{(k_{-2} + k_3)(k_{-1} + k_2[\text{B}])} \quad (6)$$

The form of this equation differs from the rate equation presented by Lammertsma and Cerfontain,<sup>17</sup> who in the denominator neglect  $k_{-2}$  in comparison to  $k_3$  in the term  $(k_{-2} + k_3)k_2[\text{B}]$ , but not in  $(k_{-2} + k_3)k_{-1}$ . No rationale was given for the partial neglect of  $k_{-2}$ , and it does not seem to simplify the kinetic analysis.



## Acknowledgements

The computational resources and services used in this work were provided by the VSC (Flemish Supercomputer Center), funded by the Hercules Foundation and the Flemish Government – department EWI. P. G. and F. D. P. wish to thank the Fund for Scientific Research – Flanders (FWO) and the Vrije Universiteit Brussel (VUB) for their continuous support. They also specifically want to mention the Strategic Research Program awarded to the ALGC group by the VUB which started on January 1, 2013.

## References

- 1 E. A. Knaggs and M. J. Nepras, in *Kirk-Othmer Encyclopedia of Chemical Technology*, John Wiley & Sons, Inc., 2000, DOI: 10.1002/0471238961.1921120611140107.a01.
- 2 M. B. Smith and J. March, in *March's Advanced Organic Chemistry*, John Wiley & Sons, Inc., 2006, DOI: 10.1002/9780470084960.ch11, pp. 657–751.
- 3 J. S. Carey, D. Laffan, C. Thomson and M. T. Williams, *Org. Biomol. Chem.*, 2006, **4**, 2337–2347.
- 4 G. P. Dado, E. A. Knaggs and M. J. Nepras, in *Kirk-Othmer Encyclopedia of Chemical Technology*, John Wiley & Sons, Inc., 2000, DOI: 10.1002/0471238961.1921120611140107.a01.pub2.
- 5 D. W. Roberts, *Org. Process Res. Dev.*, 2003, **7**, 172–184.
- 6 Y. Chen, Y. Su, F. Jiao and G. Chen, *RSC Adv.*, 2012, **2**, 5637–5644.
- 7 C. M. Suter and A. W. Weston, in *Organic Reactions*, John Wiley & Sons, Inc., 2004, vol. 3, pp. 141–197.
- 8 B. Galabov, D. Nalbantova, P. v. R. Schleyer and H. F. Schaefer, *Acc. Chem. Res.*, 2016, **49**, 1191–1199.
- 9 J. Kong, B. Galabov, G. Koleva, J.-J. Zou, H. F. Schaefer and P. v. R. Schleyer, *Angew. Chem., Int. Ed.*, 2011, **50**, 6809–6813.
- 10 B. Galabov, G. Koleva, S. Simova, B. Hadjieva, H. F. Schaefer and P. v. R. Schleyer, *Proc. Natl. Acad. Sci. U. S. A.*, 2014, **111**, 10067–10072.
- 11 G. Koleva, B. Galabov, B. Hadjieva, H. F. Schaefer and P. v. R. Schleyer, *Angew. Chem., Int. Ed.*, 2015, **54**, 14123–14127.
- 12 G. Koleva, B. Galabov, J. Kong, H. F. Schaefer and P. v. R. Schleyer, *J. Am. Chem. Soc.*, 2011, **133**, 19094–19101.
- 13 J. K. Bosscher and H. Cerfontain, *Recl. Trav. Chim. Pays-Bas*, 2010, **87**, 873–887.
- 14 J. K. Bosscher and H. Cerfontain, *Tetrahedron*, 1968, **24**, 6543–6555.
- 15 J. K. Bosscher and H. Cerfontain, *J. Chem. Soc. B*, 1968, 1524–1526, DOI: 10.1039/j29680001524.
- 16 H. Cerfontain, *Recl. Trav. Chim. Pays-Bas*, 2010, **104**, 153–165.
- 17 K. Lammertsma and H. Cerfontain, *J. Chem. Soc., Perkin Trans. 2*, 1980, 28–32, DOI: 10.1039/p29800000028.
- 18 H. Cerfontain and A. Koeberg-Telder, *Recl. Trav. Chim. Pays-Bas*, 2010, **89**, 569–574.
- 19 A. Koeberg-Telder and H. Cerfontain, *Recl. Trav. Chim. Pays-Bas*, 2010, **90**, 193–206.
- 20 J. O. Morley and D. W. Roberts, *J. Org. Chem.*, 1997, **62**, 7358–7363.
- 21 J. O. Morley, D. W. Roberts and S. P. Watson, *J. Chem. Soc., Perkin Trans. 2*, 2002, 538–544, DOI: 10.1039/b109338j.
- 22 F. H. Westheimer, *Chem. Rev.*, 1961, **61**, 265–273.
- 23 A. S. Morkovnik and A. R. Akopova, *Dokl. Chem.*, 2013, **450**, 122–126.
- 24 F. Kučera and J. Jančář, *Polym. Eng. Sci.*, 1998, **38**, 783–792.
- 25 T. M. Krygowski and M. K. Cyranski, *Phys. Chem. Chem. Phys.*, 2004, **6**, 249–255.
- 26 A. D. Becke, *Phys. Rev. A: At., Mol., Opt. Phys.*, 1988, **38**, 3098–3100.
- 27 C. Lee, W. Yang and R. G. Parr, *Phys. Rev. B*, 1988, **37**, 785–789.
- 28 S. Goedecker, M. Teter and J. Hutter, *Phys. Rev. B: Condens. Matter*, 1996, **54**, 1703–1710.
- 29 S. Grimme, J. Antony, S. Ehrlich and H. Krieg, *J. Chem. Phys.*, 2010, **132**, 154104.
- 30 B. Ensing and M. L. Klein, *Proc. Natl. Acad. Sci. U. S. A.*, 2005, **102**, 6755–6759.
- 31 G. Bussi, D. Donadio and M. Parrinello, *J. Chem. Phys.*, 2007, **126**, 014101.
- 32 J. Hutter, M. Iannuzzi, F. Schiffmann and J. VandeVondele, *Wiley Interdiscip. Rev.: Comput. Mol. Sci.*, 2014, **4**, 15–25.
- 33 A. Laio and F. L. Gervasio, *Rep. Prog. Phys.*, 2008, **71**, 126601.
- 34 A. Laio and M. Parrinello, *Proc. Natl. Acad. Sci. U. S. A.*, 2002, **99**, 12562–12566.
- 35 S. L. C. Moors, B. Brigou, D. Hertsen, B. Pinter, P. Geerlings, V. Van Speybroeck, S. Catak and F. De Proft, *J. Org. Chem.*, 2016, **81**, 1635–1644.
- 36 S. L. C. Moors, K. De Wispelaere, J. Van der Mynsbrugge, M. Waroquier and V. Van Speybroeck, *ACS Catal.*, 2013, **3**, 2556–2567.
- 37 J. Van der Mynsbrugge, S. L. C. Moors, K. De Wispelaere and V. Van Speybroeck, *ChemCatChem*, 2014, **6**, 1906–1918.
- 38 W. Humphrey, A. Dalke and K. Schulten, *J. Mol. Graphics*, 1996, **14**, 33–38, 27–38.

